5th International Workshop on
Biological Effects of Electromagnetic Fields

September 28th - October 2nd 2008, Città del Mare, Terrasini, Palermo

COMPLIANCE WITH EU BASIC RESTRICTIONS NEAR INDUCTION FURNACES USED IN PRECIOUS METAL INDUSTRY: A 3D NUMERICAL DOSIMETRIC ANALYSIS USING THE SCALAR POTENTIAL FINITE DIFFERENCE (SPFD) TECHNIQUE AND A POSTURABLE DIGITAL BODY MODEL

ZOPPETTI N., ANDREUCCETTI D.

IFAC-CNR, INSTITUTE FOR APPLIED PHYSICS "NELLO CARRARA"
VIA MADONNA DEL PIANO 10, 50019 SESTO FIORENTINO (FI) ITALY

Abstract

Induction heating is widely used for metallurgic treatments on precious metals. A survey in a few plants located in the Tuscan province of Arezzo, one of the main Italian districts of gold industry, revealed that workers involved in these treatments are often exposed to intense magnetic fields, many tens of times higher than the maximum allowable levels specified by the 2004/40/EC Directive.

A numerical approach has been developed and used to check compliance with the European Directive exposure limit values for the induced current density, as requested in these situations. This approach is based on a 3D implementation of the scalar potential finite difference method, in conjunction with an original articulation technique, able to put the digital model used to represent the exposed body in the typical posture assumed in the working practice. Thanks to the low frequency of operation and to other characteristics of induction furnaces, our approach takes great advantage of the application of the so called quasi-static approximation and of the possibility to disregard the electric component of the field.

One of the main problems we had to deal with in setting up our methods, concerned the algorithm to be used to calculated the cross-section averaged current density in the tissue of the nervous central system, as requested by the Directive. Actually, the Directive specifications are somewhat ambiguous and there are quandaries on how they should be applied. Moreover, these specifications become completely inapplicable in the general case of elliptical field polarization.

Under acceptable hypothesis, out results show that, with magnetic flux densities values exceeding up to 65 times the maximum allowed values, the averaged induced current density surpasses the exposure limit value by just a 10%, a fact that indirectly confirms the validity of the two-level approach of the Directive.

Introduction

Magnetic induction heaters are widely used in the precious metal industry for various metallurgic treatments on gold and other materials. Workers running these apparatuses are often exposed to magnetic flux densities (MFD) far more intense than the maximum field levels allowed by the 2004/40/EC Directive [1], the so called “action values”, as it also results from a survey [2] in a few plants located in the Tuscan province of Arezzo, one of the main Italian districts of gold industry.

In this work, our attention is focused on a particular case study, concerning the occupational exposure to an induction furnace operating at 3450 Hz. At this frequency, the quasi-static approximation (QSA) holds, allowing coupling to electric and magnetic fields to be computed independently [3]. Moreover, electrically induced currents have been neglected in our study, as the intensity of the electric field is far lower than the corresponding action value. This is mainly due to the low values of both the power supply voltage and the impedance of the source coil.

The exposure scenario is thus represented in figure 1, where just the source and the exposed subject are considered, while the ground and other objects are neglected. The main approximation introduced here is the removal of all conducting objects that could distort the magnetic field generated by the source. The exposed subject has extended arms, so that the edge of his fingers are less than 5 centimeters far from the source conductor.

The dosimetric analysis was carried on through the following steps.

- The exposure scenario was set up, in order to establish the exact relative positions of the source coil and the exposed subject.
- The digital body model was articulated to represent a realistic posture.
- The source was numerically modeled and the distribution of the impressed magnetic flux density was calculated in the volume occupied by the body model, in points determined by the grid adopted to discretize the problem.
- The current density distribution inside the body model was calculated using a scalar potential finite difference (SPFD) approach [4].
- The average of the current density over 1 cm^2 cross-section in the central nervous system was calculated to verify compliance with exposure limit values.

The main features of each of all these steps will be described in the following paragraphs.

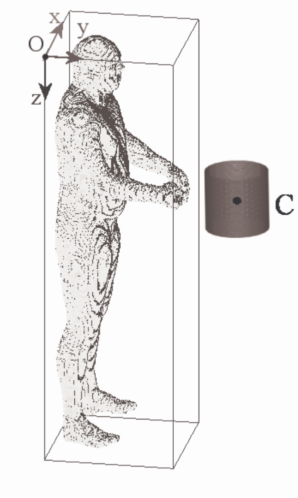

figure 1: the exposure scenario

Representation of the exposed subject

In recent years, several numerical models of the human body to be used in numerical dosimetry studies have been proposed by the scientific community [5][6][7]. These models usually put the human body in a standing posture, not able to represent the real postures occurring in occupational exposures. At IFAC-CNR an articulation algorithm was developed, that is particularly suited for use in conjunction with finite difference calculation techniques [8] and is also aimed at achieve the best compromise between accuracy and ease of applicability to different models and different joints. Currently, our model implementation is based on the Visible Human dataset [9], which has been segmented in a 3D array of 3mm x 3mm x 3mm cubic voxels. A particular tissue type – taken from a palette of about fifty different tissues – has been assigned to each voxel and tissue conductivities have been calculated at the working frequency by means of the well-known Gabriel's parametric model for the dielectric properties of body tissues [10][11][12].

In figure 2, the original model and the articulated one used in this paper are shown, with the indication of the articulated parts.

The basic steps of the articulation algorithm are as follows.

1. The body model is separated into parts.

2. Some parts are articulated, some other parts are just translated and/or rotated, the remaining parts are left unchanged; the articulation process exploits the elasticity of the fleshy parts, while bones are not deformed.
3. The rotated and articulated parts need to be re-sampled, so that the constraint of cubic voxels is satisfied.
4. The modified parts are put together to form the articulated body model; correct reconstruction of the articulated body can be carried on thanks to the imposed constraint that voxels lying on transition sections that separate different parts are not deformed.

The re-sampling process (3) is a critical step from the point of view of mass conservation of the body model; in the present case study, the articulated body model mass resulted 0.39% (0,4 kg) higher than the original one.
Another aspect to be appointed to, concerns the rendering of tissue elasticity, which is simplified so that the system of equations to be solved becomes linear and has separate coordinates. These approximations are particularly critical for the articulation of the shoulder, that in consequence has to be limited to an angle of 30 degrees with respect to the initial posture.

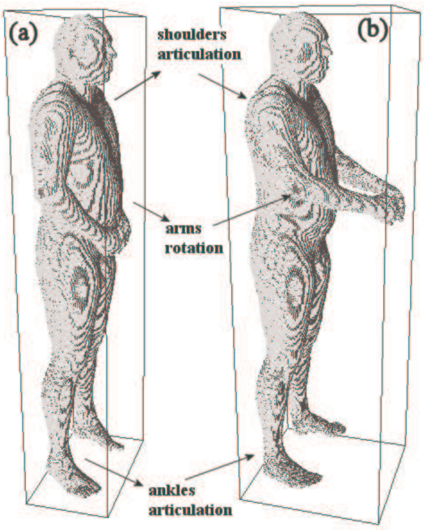

figure 2: digital body model; (a) original posture (VHP), (b) articulated posture.

Source modeling

The magnetic flux density B generated by a current-carrying conductor, like a solenoid-shaped coil (figure 3), can be calculated by numerically integrating the Biot-Savart law in differential form along the current path Γ, as shown in eq. 1. The SPFD method requires the source to be characterized through the magnetic vector potential A instead: this can be accomplished by using eq. 2.
Dimensions of the solenoid (diameter and height of the cylinder) and current intensity I were set according to the technical documentation of the furnace, supplied by the manufacturer.

$$\vec{B}(Q) = \frac{\mu_0 I}{4\pi} \int_{P \in \Gamma} \frac{dP \times (Q - P)}{|Q - P|^3} \qquad \text{eq. 1}$$

$$\vec{A}(Q) = \frac{\mu_0 I}{4\pi} \int_{P \in \Gamma} \frac{dP}{|Q - P|} \qquad \text{eq. 2}$$

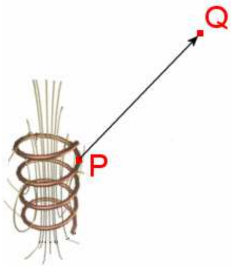

figure 3: calculation of the MFD or the magnetic vector potential by means of a line integral along the solenoid

The number of turns and the exact position of the solenoid inside the apparatus were adjusted in order to obtain the best fit between calculated and measured MFD values. The position of measurement points is indicated in figure 4, while measured and calculated values are showed in figure 5.

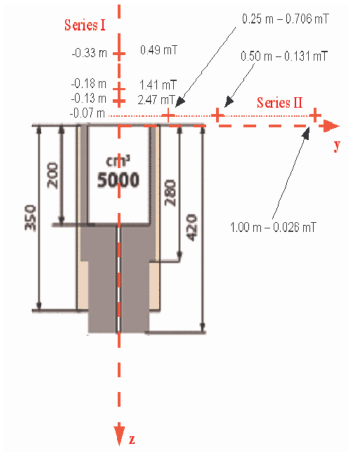

figure 4: furnace schematic diagram and position of measurement points

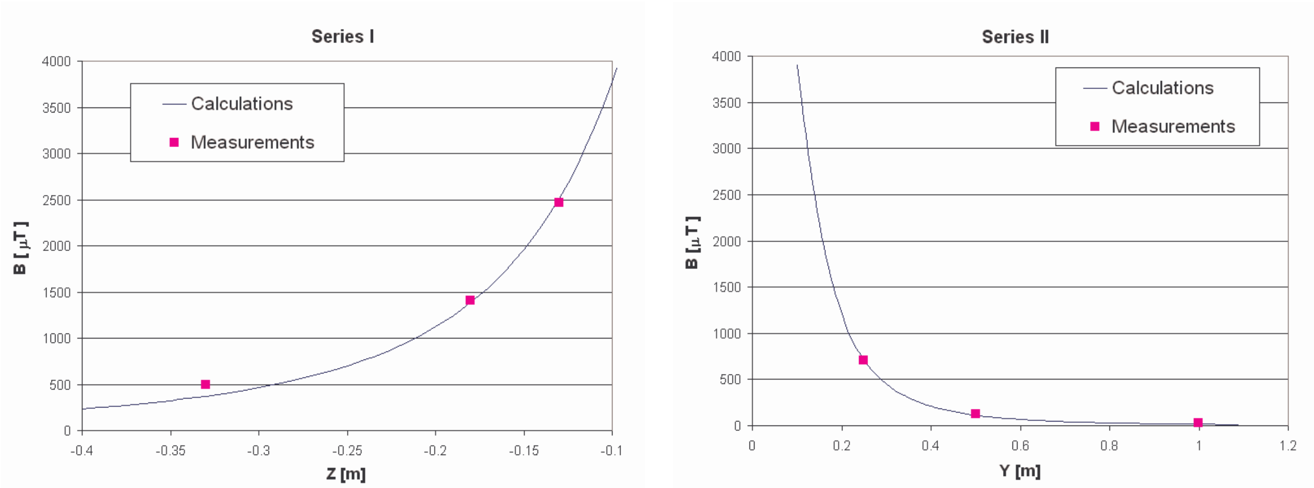

figure 5: comparison of measured and calculated MFD values

Numerical method

An implementation of the SPFD method [13][14] was used to calculate the magnetically induced current density inside the body model. Several considerations supported this choice. First of all, the SPFD, like all finite difference methods, is particularly appropriate to cope with digital models segmented in cubic voxels. Furthermore, the method is well-suited for the solution of 3D problems, because it always leads to a scalar equation. Lastly, the SPFD method – though valid in general – gives rise, in quasi-static conditions, to equations that can be solved very easily. In this case in fact, the vector potential A can be assumed known and consisting of just the potential $\underline{A}_{source}$ generated by the source and calculated by means of eq. 2. The unique unknown, in this case, is the scalar potential φ and the basic SPFD differential equation becomes:

$$\nabla \cdot \left[\sigma\left(-\nabla\varphi - j\omega\vec{A}_{source}\right)\right] = 0 \qquad \text{eq. 3}$$

In eq. 3, the electrical permittivities of biological tissues are neglected, since at low frequencies conduction currents prevail over displacement currents. Strictly speaking, this condition (which is often considered part of the QSA) is valid up to a few hundred kilohertz, even if it is often applied up to 1 MHz and more.

Once this equation has been solved and the scalar potential determined, the internal electric field $\underline{E}_i$ and the current density $\underline{J}$ can be calculated with the following expressions:

$$\vec{E}_i = -\nabla\varphi - j\omega\vec{A}_{source} \quad \Rightarrow \quad \vec{J} = \sigma\vec{E}_i = \sigma\left(-\nabla\varphi - j\omega\vec{A}_{source}\right) \qquad \text{eq. 4}$$

As the magnetic field only is considered, no supplementary boundary conditions are needed, since the SPFD equation is a particular formulation of the current continuity principle.

The computer program that implements the method solves, by means of a standard matrix-free iterative technique, the linear system obtained by applying eq. 3 to all the voxels (more than 3.000.000) that composes the digital body model.

Cross-section averaging of current density

To verify compliance with exposure limit values, current densities have to be averaged in every voxel over a cross-section of 1 cm^2, as it is prescribed by Note 3 of Table 1 of the 2004/40 Directive ("*Because of the electrical inhomogeneity of the body, current densities should be calculated as averages over a cross-section of 1 cm^2 perpendicular to the current direction*"). Also important, the "target tissues" for this averaging are the tissues of the central nervous system (CNS), as Note 2 of the same table specifies that "*The exposure limit values on the current density are intended to protect against acute exposure effects on central nervous system tissues in the head and trunk of the body*".

Dawson et al. [15] introduced a simplified algorithm for current density averaging. According to it: "*the components of the current density average associated with a given voxel are computed by averaging the perpendicular components of current density over squares with 1 cm edges centered on the voxel and parallel to the three principal Cartesian planes. The resulting vector field is treated similar to the current density itself in dosimetry computations*".

This algorithm introduces two main approximations. First, it uses square cross-sections that intersect different portions of surrounding voxels, depending from their orientations. Second and more important, the cross-sections used to average the current density are not necessarily perpendicular to the current direction, as required by the Directive. In the following, we will refer to this algorithm as "Dawson's simplified averaging algorithm".

The Dawson's simplified algorithm gives exact results in case of a uniform vector field, but is less indicated in case of non uniform current density distribution, like the present one. For this reason, we developed an algorithm that implements the exact geometrical definition of the cross-section averaging of a vector field. This algorithm – which will be called "exact geometrical averaging algorithm" downward – consists in the following steps for each voxel where the average has to be calculated.

- A plane ("averaging plane") is chosen that is perpendicular to the current density in the considered voxel (the "application point" of the average).
- The circular 1 cm^2 cross-section that lies on the averaging plane and has center in the application point is considered.
- The intersecting section S_i of every voxel with the circular cross-section of the previous step is determined. Since the averaging plane is not necessarily perpendicular to a voxel face, this intersecting section can assume the form of a generic polygon with 3,4,5 or 6 edges ([16], figure 6).
- The cross-section average of current density is calculated in every voxel according to eq. 5.

$$J_S = \frac{\sum_{i=1}^{N}\left[S_i\left(\vec{J}_i \cdot \vec{V}\right)\right]}{\sum_{i=1}^{N} S_i} \qquad \text{eq. 5}$$

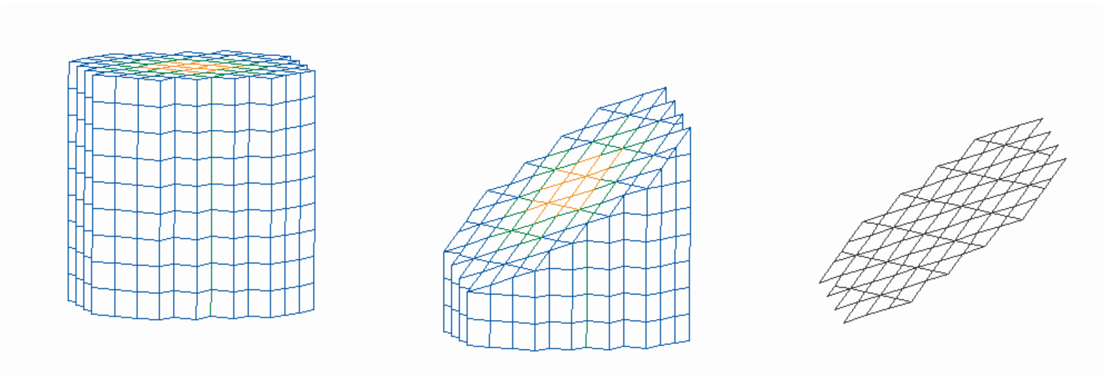

figure 6: plane sections of a cubic voxel structure

The averaging algorithm presented here is easily applicable in case of impressed fields and current densities with linear polarization, like in the present case. The concept of cross-section perpendicular to a vector with elliptic or circular polarization is not well defined and the choice of the cross-section orientation is arbitrary.

It should be noted that the Dawson's simplified algorithm is directly applicable also to circular or elliptical polarizations, thanks to the fact that averaging cross-sections are parallel to the three main coordinate planes and are not linked to the actual current density orientation.

Limitation to central nervous system

When the application point of the averaging cross-section is close to a surface separating an organ of the CNS from a different tissue, the averaging cross-section will possibly intersect voxels that do not belong to the CNS. For instance, the spinal chord (or the structure composed by the spinal chord and the cerebro-spinal fluid) has in many cases a cross section smaller than 1 cm^2. In these situations, it should be decided if the contributes to the average coming from tissues not belonging to the CNS have to be considered.

Different approaches have been presented in literature, in past [15] and more recent works [17][18][19]. In this paper, we adopted the so called "full-averaging" algorithm [15], according to which the averaging application point is always taken in a voxel that belongs to the central nervous system, but the contributes of all other voxels (even not belonging to the CNS) that intersect the averaging plane are also fully considered. This choice is inspired by Note 3 of Table 1 of the Directive, that introduces the current density averaging "*because of the electrical inhomogeneity of the body*". If the aim of the averaging is to take into account of the electrical inhomogeneity, it seems a nonsense to exclude some voxels once the averaging cross-section has been defined.

Results

At the operating frequency of the source (3450 Hz), the action value for the MFD is 30.7 µT and the exposure limit value for the current density is 34.5 mA/m^2. As it can be seen in figure 7 and figure 8, the MFD largely exceeds the action value. In proximity of the source, where the worker puts his hands, the intensity of the MFD is higher than 2 mT; in the front part of the trunk, it is still over 100 µT.

In figure 9, figure 10 and figure 11, the distribution of the RMS current density in every voxel (local peak value) is shown respectively on a sagittal, coronal and axial section. In figure 12, details of the same distribution are given inside the right arm of the exposed subject.

In all these figures, it can be noted that the current density tends to be more intense on the peripheral of the body and where the body cross-section on a plane perpendicular to the magnetic field is larger. Obviously, current density tends also to flow where the tissue conductivity is higher.

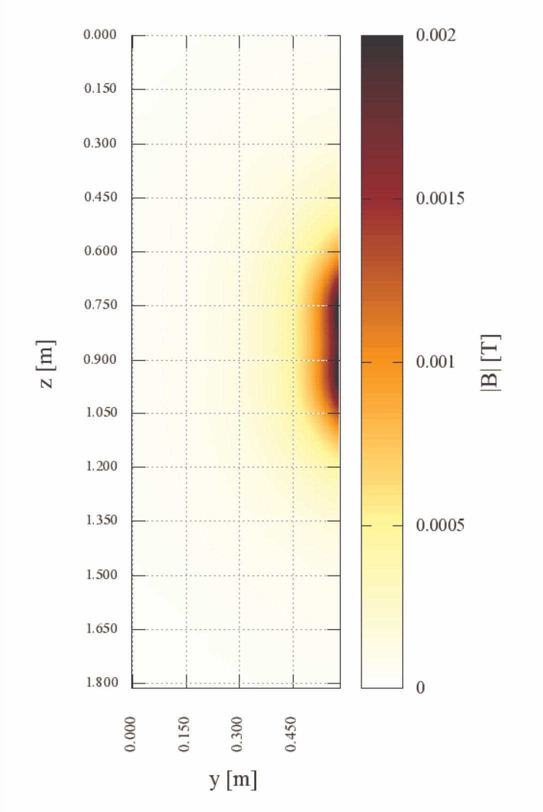

figure 7: MFD RMS values on a median sagittal body cross section

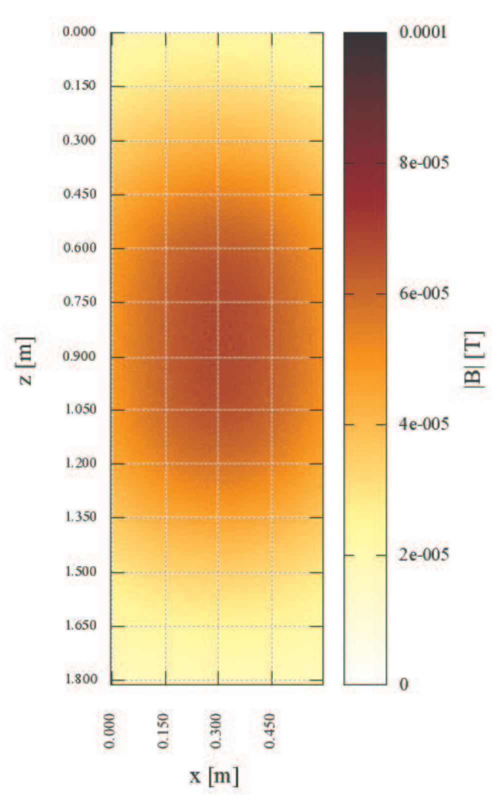

figure 8: MFD RMS values on a median coronal body cross section

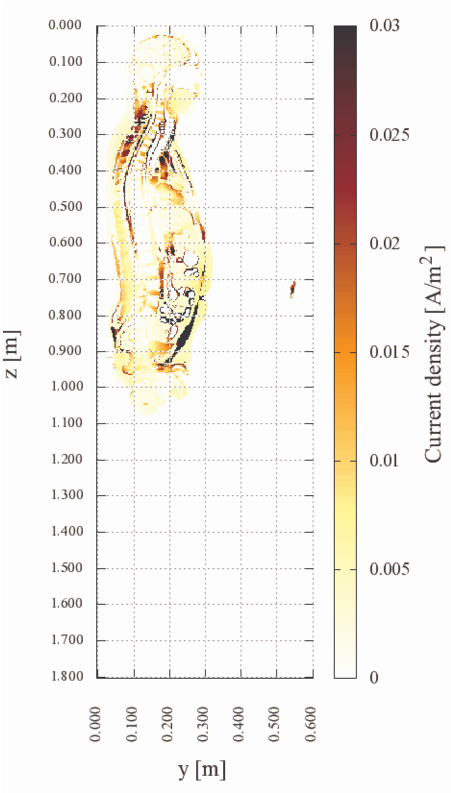

figure 9: local peak value of the RMS current density on the sagittal body cross section of figure 7

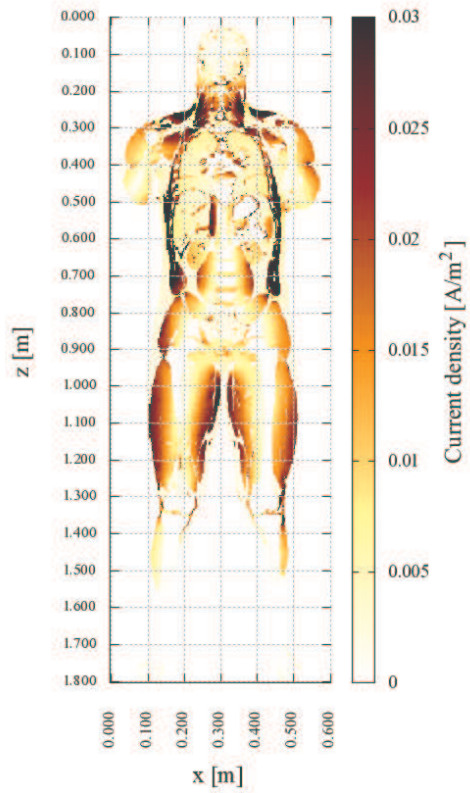

figure 10: local peak value of the RMS current density on the coronal body cross section of figure 8

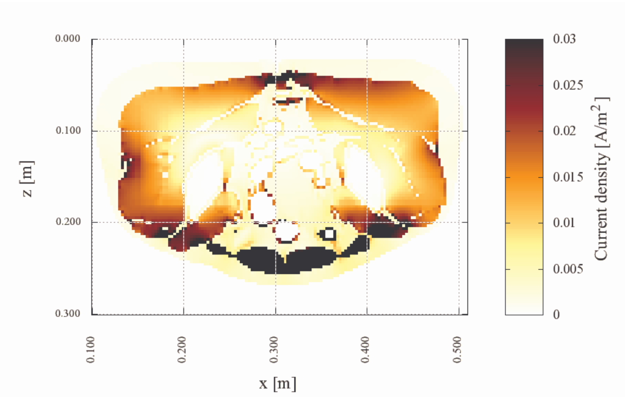

figure 11: local peak value of the RMS current density on an axial body cross section in the chest region

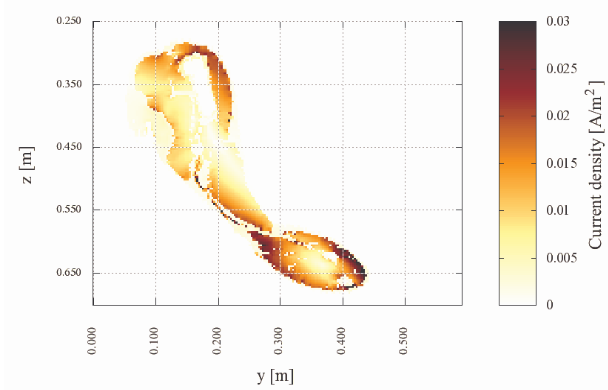

figure 12: local peak value of the RMS current density on a sagittal body cross section in the right arm region

Two aspects that deserve further research should be clearly underlined at this point.

- First of all, it should be definitely decided if the cerebro-spinal fluid (CSF) has to be considered a "target tissue" for the application of the exposure limit values. Even if it is not properly a nervous structure, it is formally part of the CNS, as it is reported in many anatomic atlases. In the scientific literature, some dosimetric studies consider the CSF as a target tissue [15], but some other do not [17] [18]. As it can be seen in the following table, this choice has a great relevance in term of compliance with exposure limit values, since the cerebro-spinal fluid is one of the more conductive tissues in the body. Conductivity values at 3450 Hz listed in table 1 are calculated using the cited C.Gabriel's parametric model for the dielectric properties of tissues.

Tissue	Conductivity [S/m]
Brain gray matter	0.1067
Brain white matter	0.0655
Cerebellum	0.1267

Cerebro spinal fluid	2.0000
Nerve & spinal chord	0.0320
Fat	0.0234
Heart	0.1277
Muscle	0.3341
Tendon	0.3854

table 1: samples of tissue conductivities at 3450 Hz

- In the digital body model used in this work, the spinal chord and the nerves are not distinguishable. To obtain a more detailed analysis, peripheral nerves and spinal chord should be separated.

A detailed analysis of what happens in terms of peak and cross-section averaged current densities is reported in the following tables. table 2 refers to the local peak (i.e. not cross-section averaged) values of current density in the tissues of the CNS; the maximum, the mean and the 99 percentile calculated on all the voxels made up by the considered tissues are listed in each row. In table 3, results of the same analysis are reported for four different tissues.

	max [mA/m^2]	mean [mA/m^2]	99% [mA/m^2]
Brain gray matter	7.59	1.87	4.68
Brain white matter	4.19	1.34	2.88
Cerebellum	11.00	2.48	6.86
Cerebro spinal fluid	112.79	19.97	64.70
Nerve & spinal chord	19.29	1.85	10.02

table 2: local peak value of the RMS current density in the CNS voxels

	max [mA/m^2]	mean [mA/m^2]	99% [mA/m^2]
Fat	91.82	2.20	7.73
Heart	17.89	4.13	9.27
Muscle	235.13	15.98	59.34
Tendon	280.11	15.16	84.02

table 3: local peak value of the RMS current density in some non-CNS voxels

In table 4, the maximum, the mean and the 99 percentile of the 1 cm^2 cross-section-averaged current density values, calculated using the exact geometrical averaging algorithm, are reported. These values are calculated on all the voxels belonging to the CNS.

	max [mA/m^2]	mean [mA/m^2]	99% [mA/m^2]
Brain gray matter	12.51	2.59	7.50
Brain white matter	8.97	1.70	4.53
Cerebellum	16.11	2.89	11.09
Cerebro spinal fluid	32.84	8.02	25.95
Nerve & spinal chord	38.15	5.56	19.81

table 4: 1 cm^2 averaged RMS current density
(exact geometrical – full tissue averaging algorithms)

In table 5 the same analysis of table 4 is repeated, considering the Dawson’s simplified averaging algorithm instead.

	max [mA/m^2]	mean [mA/m^2]	99% [mA/m^2]
Brain gray matter	7.71	2.15	5.03
Brain white matter	4.96	1.49	3.26
Cerebellum	9.58	2.66	7.79
Cerebro spinal fluid	77.89	15.63	48.01
Nerve & spinal chord	19.10	3.26	11.83

table 5: 1 cm^2 averaged RMS current density
(Dawson’s simplified – full tissue averaging algorithms)

The columns reporting maximum values are particularly important, since these are the numbers that should be compared with the exposure limit values to verify the compliance with the 2004/40 CE Directive. As it can be noted, the cross-section average calculated using the exact geometrical averaging algorithm is not compliant with the exposure limit value of 34,5 mA/m^2 in nervous tissue. Using the Dawson's simplified algorithm, the overcoming of exposure limit value takes place in the CSF.

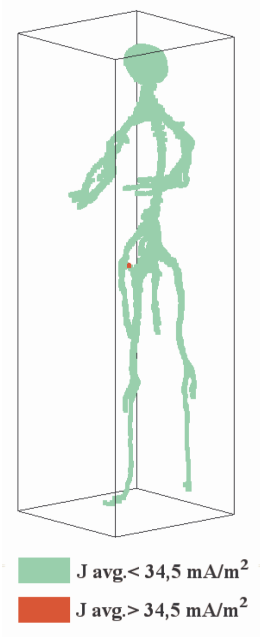

figure 13 1 cm^2 averaged RMS current density **Javg** (exact geometrical – full tissue averaging algorithms) in CNS

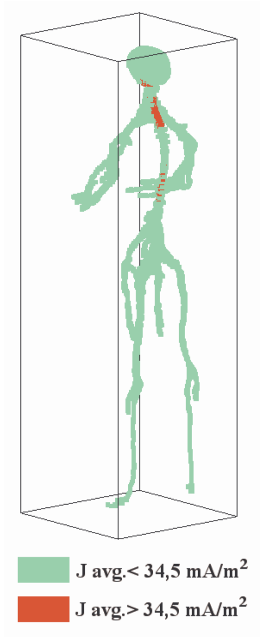

figure 14 1 cm^2 averaged RMS current density **Javg** (Dawson's simplified – full tissue averaging algorithms) in CNS

figure 13 and figure 14 show that, while using our exact geometrical algorithm the maximum is reached in the peripheral nerves of the pelvis region, using the Dawson's simplified one the maximum is reached in the cerebro-spinal fluid surrounding the spinal chord.

Summary and conclusions

The problem of checking compliance with exposure limit values defined in the 2004/40/CE Directive was presented in the case of an induction furnace used in gold industry.

The main steps of the analysis were illustrated and discussed, underlying the open problems on which further research is needed. The key points of our analysis are the method used to articulate the body model and the introduction of a exact algorithm for the cross-section averaging of the current density.

The results show that, with a MFD exceeding more than 65 times the corresponding action value, the averaged current density surpasses its exposure limit value by just a 10%. This fact, that indirectly confirms the validity of the two-level approach of the Directive, is due to the magnetic field being highly non-homogeneous in the body volume.

The problem of the cross-section averaging algorithm is particularly delicate, considering that it produces the value to be compared with the exposure limit. In this respect, two aspects dealing with the interpretation of the Directive were pointed out: the case of the CSF tissue to be or not considered part of the CNS and the problem of cross-section averaging of a vector field with circular or elliptic polarization.

References

[1] Directive 2004/40/EC of the European Parliament and of the Council of 29 April 2004 on the minimum health and safety requirements regarding the exposure of workers to the risks arising from physical agents (electromagnetic fields). Official Journal of the European Union, L 184, 24 May 2004.

[2] D.Andreuccetti, M.Bini, A.Ignesti, R.Olmi e R.Vanni. *Campi elettrici e magnetici dispersi da apparati ad induzione per l'industria orafa*. Atti della VIII riunione nazionale di Elettromagnetismo Applicato, Capri (NA), Ottobre 1990, pag.477-480 (in Italian).

[3] D.Andreuccetti and N.Zoppetti. *Quasi-static electromagnetic dosimetry: from basic principles to examples of applications*. International Journal of Occupational Safety and Ergonomics (JOSE), Vol. 12, No. 2 (2006), pp.201-215.

[4] H.R.Chuang and K.M.Chen. *A numerical method for the computation of induced currents inside 3-D heterogeneous biological bodies by ELF-LF electric fields*. IEEE Transactions on Biomedical Engineering, Vol.BME-36, N.6 (June 1989), pp.628-634.

[5] P.J.Dimbylow. *The development of realistic voxel phantoms for electromagnetic field dosimetry*. Proceedings of the International Workshop on Voxel Phantom Development (National Radiological Protection Board Report, 1996), pp.1-7.

[6] P.J.Dimbylow. *Development of the female voxel phantom, NAOMI, and its application to calculations of induced current densities and electric fields from applied low frequency magnetic and electric fields*. Physics in Medicine and Biology, Vol.50 (2005), pp.1047–1070.

[7] P.J.Dimbylow. *Development of pregnant female, hybrid voxel-mathematical models and their application to the dosimetry of applied magnetic and electric fields at 50Hz*. Physics in Medicine and Biology, Vol.51 (2006), pp.2383–2394.

[8] N.Zoppetti e D.Andreuccetti. *Un algoritmo per l'articolazione di modelli digitali dell'organismo umano mirato all'utilizzo di metodi alle differenze finite per la dosimetria numerica dei campi elettromagnetici*. Atti del Convegno Nazionale dBA-2006 su "Rumore, vibrazioni, microclima, campi elettromagnetici, radiazioni ottiche e ionizzanti - Valutazione, prevenzione e bonifica negli ambienti di lavoro", Modena, 12-13 ottobre 2006, Vol.3, pag.83-96 (in Italian).

[9] U.S. National Library of Medicine. *The Visible Human Project ®*. Internet resource at http://www.nlm.nih.gov/research/visible/visible_human.html

[10] C.Gabriel et al. *The dielectric properties of biological tissues (part I, II and III)*. Physics in Medicine and Biology, Vol.41 (1996), pp.2231-2293.

[11] C.Gabriel and S.Gabriel. *Compilation of the Dielectric Properties of Body Tissues at RF and Microwave Frequencies*. http://niremf.ifac.cnr.it/docs/DIELECTRIC/home.html

[12] Institute for Applied Physics "Nello Carrara" (IFAC) of the Italian National Research Council (CNR). *Dielectric Properties of Body Tissues*. http://niremf.ifac.cnr.it/tissprop/

[13] K.R.Davey, C.H.Cheng and C.M.Epstein. *Prediction of magnetically induced electric fields in biological tissue*. IEEE Transactions on Biomedical Engineering, Vol.BME-38, No.5 (May 1991), pp.418-422.

[14] P.J.Dimbylow. *Induced current densities from low-frequency magnetic fields in a 2 mm resolution, anatomically realistic model of the body*. Physics in Medicine and Biology, Vol.43 (1998), pp.221-230.

[15] T.W.Dawson, K.Caputa and M.Stuchly. *Magnetic field exposures for UK live-line workers*. Physics in Medicine and Biology, Vol.47 (2002), pp.995-1012

[16] JP.Reveill`es. *The Geometry of the Intersection of Voxel Spaces*. Electronic Notes in Theoretical Computer Science 46 (2001). http://www.elsevier.nl/locate/entcs/volume46.html

[17] A.Bahr, T.Bolz and C.Hennes. *Numerical dosimetry ELF: accuracy of the method, variability of models and parameters, and the implication for quantifying guidelines*. Health Physics, Vol 92, N.6 (June 2007), pp.521-530.

[18] P.Dimbylow. *Quandaries in the application of the ICNIRP low frequency basic restriction on current density*. Physics in Medicine and Biology. Vol.53 (2008), pp.133–145.

[19] S.Crozier, H.Wang, A.Trakic and F.Liu. *Exposure of workers to pulsed gradients in MRI*. Journal of Magnetic Resonance Imaging, Vol.26 (2007), pp.1236–1254.